Neurotherapeutics (2019) 16:216–230
https://doi.org/10.1007/s13311-018-0665-9

ORIGINAL ARTICLE

Inhibition of miR-155 Limits Neuroinflammation and Improves Functional Recovery After Experimental Traumatic Brain Injury in Mice

Rebecca J. Henry[1] · Sarah J. Doran[1] · James P. Barrett[1] · Victoria E. Meadows[1] · Boris Sabirzhanov[1] · Bogdan A. Stoica[1] · David J. Loane[1,2] · Alan I. Faden[1,3]

Published online: 17 September 2018

Abstract

Micro-RNAs (miRs) are short, noncoding RNAs that negatively regulate gene expression at the post-transcriptional level and have been implicated in the pathophysiology of secondary damage after traumatic brain injury (TBI). Among miRs linked to inflammation, miR-155 has been implicated as a pro-inflammatory factor in a variety of organ systems. We examined the expression profile of miR-155, following experimental TBI (controlled cortical impact) in adult male C57Bl/6 mice, as well as the effects of acute or delayed administration of a miR-155 antagomir on post-traumatic neuroinflammatory responses and neurological recovery. Trauma robustly increased miR-155 expression in the injured cortex over 7 days. Similar TBI-induced miR-155 expression changes were also found in microglia/macrophages isolated from the injured cortex at 7 days post-injury. A miR-155 hairpin inhibitor (antagomir; 0.5 nmol), administered intracerebroventricularly (ICV) immediately after injury, attenuated neuroinflammatory markers at both 1 day and 7 days post-injury and reduced impairments in spatial working memory. Delayed ICV infusion of the miR-155 antagomir (0.5 nmol/day), beginning 24 h post-injury and continuing for 6 days, attenuated neuroinflammatory markers at 7 days post-injury and improved motor, but not cognitive, function through 28 days. The latter treatment limited NADPH oxidase 2 expression changes in microglia/macrophages in the injured cortex and reduced cortical lesion volume. In summary, TBI causes a robust and persistent neuroinflammatory response that is associated with increased miR-155 expression in microglia/macrophages, and miR-155 inhibition reduces post-traumatic neuroinflammatory responses and improves neurological recovery. Thus, miR-155 may be a therapeutic target for TBI-related neuroinflammation.

Key Words Traumatic brain injury · miR-155 · microglial activation · neuroinflammation · neuroprotection

David J. Loane and Alan I. Faden contributed equally to this work.

✉ David J. Loane
dloane@som.umaryland.edu

✉ Alan I. Faden
afaden@som.umaryland.edu

Rebecca J. Henry
rhenry@som.umaryland.edu

Sarah J. Doran
sarah.doran@som.umaryland.edu

James P. Barrett
jbarrett@som.umaryland.edu

Victoria E. Meadows
vmeadows@som.umaryland.edu

Boris Sabirzhanov
bsabirzhanov@som.umaryland.edu

Bogdan A. Stoica
bstoica@som.umaryland.edu

[1] Department of Anesthesiology and Shock, Trauma and Anesthesiology Research (STAR) Center, University of Maryland School of Medicine, Baltimore, MD, USA

[2] Department of Anesthesiology, University of Maryland School of Medicine, 655 West Baltimore Street, No. 6-011, Baltimore, MD 21201, USA

[3] Department of Anesthesiology, University of Maryland School of Medicine, 685 West Baltimore Street, MSTF No. 6-02, Baltimore, MD 21201, USA

Introduction

Micro-RNAs (miRs) are small (23 nucleotides) noncoding RNAs that regulate gene expression at a post-translational level by binding to the 3′-untranslated region (UTR) of target messenger RNAs (mRNAs), thereby leading to their degradation and/or translational inhibition [1]. Among the numerous miRs, miR-155 has been extensively studied and has been implicated in inflammatory-associated processes (for review, see Dickey et al. [2], Ponomarev et al. [3], and Quinn and O'Neill [4]). Specifically, miR-155 is upregulated in activated microglia and macrophages, serving to drive these cells towards a pro-inflammatory phenotype [5]. In microglia, knockdown of miR-155 by hairpin inhibitors (antagomirs) reduces the release of inflammatory mediators, including nitric oxide and pro-inflammatory cytokines [e.g., interleukin-1β (IL-1β), tumor necrosis factor-α (TNFα)], and attenuates microglial cell-mediated neurotoxicity [6]. Furthermore, miR-155 has been shown to be involved in chemokine signaling, both in the periphery [7–10] and within the central nervous system (CNS) [11]. Inhibition of miR-155 can attenuate toxic neuroinflammatory responses in the CNS [12–14] and improves neurological recovery in experimental models of multiple sclerosis (MS) [15], amyotrophic lateral sclerosis (ALS) [16], neuropathic pain [14], spinal cord injury (SCI) [12], Parkinson's disease (PD) [17], and ischemic stroke [13, 18].

Recent studies from our group, and others, demonstrate that experimental traumatic brain injury (TBI) increases expression of miR-155 in the injured cortex and hippocampus [19, 20]. Moreover, such injuries induce microglial cell-mediated neuroinflammatory responses that are associated with neuronal loss and persistent neurological impairments [21, 22]. Given the documented pro-inflammatory role of miR-155 in neurodegenerative diseases, TBI-induced alteration of miR-155 in microglia may contribute to chronic neuroinflammation and related neurodegeneration. The aims of the present study were to 1) investigate the temporal profile of miR-155 expression in the injured cortex following experimental TBI in relation to microglial/macrophage activation and 2) evaluate the therapeutic potential of inhibiting miR-155 following TBI on long-term neuroinflammatory and neurobehavioral responses. We performed 2 molecular intervention studies using specific miR-155 hairpin inhibitors (antagomirs) that were delivered ICV either immediately after controlled cortical impact (CCI) in adult male C57Bl/6J mice or beginning at 24 h by continuous infusion using mini-osmotic pumps. Molecular, histological, and neurobehavioral outcome measures were used to examine the effects of inhibiting miR-155 on post-traumatic neuroinflammatory responses and neurological recovery.

Methods

Animals

Studies were performed using adult male C57Bl/6J mice (10–12 weeks old) (Taconic Biosciences, Inc., Germantown, NY). Mice were housed in the animal care facility at the University of Maryland, School of Medicine, under a 12-h light–dark cycle, with ad libitum access to food and water. All surgical procedures were carried out in accordance with protocols approved by the Institutional Animal Care and Use Committee (IACUC) at the University of Maryland School Of Medicine.

Study 1

Sham and CCI C57Bl/6J mice were anesthetized (100 mg/kg sodium pentobarbital, I.P.) at 1 h, 24 h, 72 h, and 7 days post-injury ($n = 6$/group) and transcardially perfused with ice-cold 0.9% saline (100 ml). Ipsilateral cortical tissue was rapidly dissected and snap-frozen on liquid nitrogen for RNA extraction. In a separate cohort of mice, sham and CCI C57Bl/6J mice were anesthetized (100 mg/kg sodium pentobarbital, I.P.) at 7 days post-injury ($n = 6$/group) and transcardially perfused with ice-cold 0.9% saline (100 ml). Ipsilateral cortical tissue was rapidly dissected and processed for cluster of differentiation 11b-positive selection of microglia/macrophages using MACS Separation Technology (Miltenyi Biotec, Auburn, CA) and snap-frozen on liquid nitrogen for RNA extraction.

Study 2

CCI C57Bl/6J mice ($n = 5$–6/group) received a single ICV injection of miR-155 antagomir or negative control antagomir at 15 min post-injury. Sham-injured C57Bl/6J mice served as controls. At 24 h following injury, mice were anesthetized (100 mg/kg sodium pentobarbital, I.P.) and transcardially perfused with ice-cold 0.9% saline (100 ml), and ipsilateral cortical tissue was rapidly dissected and snap-frozen on liquid nitrogen for RNA extraction and protein analysis.

Study 3

CCI C57Bl/6J mice ($n = 8$/group) received a single ICV injection of miR-155 antagomir or negative control antagomir at 15 min post-injury. Sham-injured C57Bl/6J mice served as controls. Spatial working memory was assessed using a Y-maze test at 7 days post-injury, immediately prior to euthanasia. Mice were anesthetized (100 mg/kg sodium pentobarbital, I.P.) and transcardially perfused with ice-cold 0.9% saline (100 ml), and ipsilateral hippocampal tissue was rapidly dissected and snap-frozen on liquid nitrogen for RNA extraction.

Study 4

CCI C57Bl/6J mice ($n = 6–7$/group) received a delayed continuous 6-day ICV infusion of miR-155 antagomir or negative control antagomir, via a mini-osmotic pump, beginning at 24 h post-injury. Sham-injured C57Bl/6J mice served as controls. At 7 days post-injury, mice were anesthetized (100 mg/kg sodium pentobarbital, I.P.) and transcardially perfused with ice-cold 0.9% saline (100 ml). Ipsilateral hippocampal tissue was rapidly dissected and snap-frozen on liquid nitrogen for RNA extraction.

Study 5

CCI C57Bl/6J mice ($n = 12–15$/group) received a delayed continuous 6-day ICV infusion of miR-155 antagomir or negative control antagomir, via a mini-osmotic pump, beginning at 24 h post-injury. Sham-injured C57Bl/6 mice served as controls. Motor function was assessed using the beam walk test on post-injury days (PIDs) 1, 3, 5, 7, 14, 21, and 28. Cognitive function was assessed using the Y-maze (spatial working memory; PID 11). At 28 days post-injury, mice were anesthetized (100 mg/kg sodium pentobarbital, I.P.) and transcardially perfused with ice-cold 0.9% saline (100 ml), followed by 300 ml of 4% paraformaldehyde. Brains were removed and post-fixed in 4% paraformaldehyde overnight, cryoprotected in 30% sucrose, and were processed for histological outcome measures.

Controlled Cortical Impact

Our custom-designed CCI injury device consists of a microprocessor-controlled pneumatic impactor with a 3.5-mm-diameter tip. Mice were anesthetized with isoflurane evaporated in a gas mixture containing 70% N_2O and 30% O_2 and administered through a nose mask (induction at 4% and maintenance at 2%). Depth of anesthesia was assessed by monitoring respiration rate and pedal withdrawal reflexes. Mice were placed on a heated pad, and core body temperature was maintained at 37 °C. The head was mounted in a stereotaxic frame, and the surgical site was clipped and cleaned with Nolvasan and ethanol scrubs. A 10-mm midline incision was made over the skull, the skin, and fascia were reflected, and a 4-mm craniotomy was made on the central aspect of the left parietal bone. The impounder tip of the injury device was then extended to its full stroke distance (44 mm), positioned to the surface of the exposed dura, and reset to impact the cortical surface. Moderate-level CCI was induced using an impactor velocity of 6 m/s and a deformation depth of 2 mm as previously described [22, 23]. After injury, the incision was closed with interrupted 6-0 silk sutures, anesthesia was terminated, and the animal was placed into a heated cage to maintain its normal core temperature for 45 min post-injury. Sham animals underwent the same procedure as TBI mice except for the impact.

Molecular Interventions

Acute ICV Administration

At 15 min post-injury, mice received a single ICV injection of miR-155 antagomir (0.5 nmol; GE Dharmacon, Lafayette, CO) or negative control antagomir (equal concentration; GE Dharmacon). All drugs were made up in artificial cerebrospinal fluid (aCSF) and were injected into the left lateral ventricle (coordinates from the bregma: posterior, − 0.5 mm; lateral, + 1.5 mm; ventral, − 2.0 mm) using a 30-gauge needle attached to a Hamilton syringe at a rate of 0.5 ml/min, with a final volume of 5 μl.

Delayed Continuous ICV Administration

Immediately prior to CCI, the right lateral ventricle was stereotaxically perforated with brain infusion kit 3 (ALZET, DURECT Corporation, Cupertino, CA; coordinates from the bregma: posterior, − 0.7 mm; lateral, − 1.5 mm; ventral, − 2.0 mm). At 24 h after moderate-level CCI on the left parietal cortex, the infusion cannula was connected to a mini-osmotic pump (ALZET; pump model 1007D) that was implanted subcutaneously in the animal's back, just behind the scapula. Osmotic pumps were primed for ~8 h prior to implantation and were filled with miR-155 antagomir (0.5 nmol/day) or equal concentration of negative control antagomir. Once implanted, the pumps continually infused miR-155 antagomir or negative control antagomir for 6 days at a rate of 0.5 μl/h.

Isolation of Cluster of Differentiation 11b-Positive Cells

A magnetic bead-conjugated anti-cluster of differentiation 11b (CD11b) was used to isolate microglia/macrophages from ipsilateral cortical tissue using MACS Separation Technology (Miltenyi Biotec, Auburn, CA) as previously described [24]. Briefly, ipsilateral cortical tissues from sham and CCI mice were rapidly microdissected and a single cell suspension was prepared using enzymatic digestion (Neural Tissue Dissociation Kit; Miltenyi Biotec) in combination with a gentleMACS Dissociator. Myelin was removed using Myelin Removal Beads II and LS columns (Miltenyi Biotec), and cells were incubated with anti-CD11b MicroBeads (Miltenyi Biotec) and loaded onto a MS column (Miltenyi Biotec) placed in the magnetic field of a MACS separator. The negative fraction (flow through) was collected, and the column was washed 3 times with MACS buffer (Miltenyi Biotech). CD11b-positive cells were eluted by removing the magnetic field, resulting in the isolation of viable

CD11b-positve cells (microglia/macrophages) from sham and CCI mice. Cells were snap-frozen on liquid N_2 for RNA extraction.

Real-Time PCR

Total RNA was extracted from the ipsilateral cortex and hippocampus of sham and CCI mice using a miRNeasy isolation kit (Qiagen, Valencia, CA) with on-column DNase treatment (Qiagen).

mRNA Expression

Complementary DNA (cDNA) synthesis was performed on 1 μg of total RNA using a Verso cDNA RT kit (Thermo Scientific, Pittsburg, PA); the protocols used were per the manufacturer's instructions. Real-time PCR for target mRNAs was performed using TaqMan gene expression assays [NADPH oxidase 2 (NOX2), Mm01287743_m1; human neutrophil cytochrome b light chain ($p22^{phox}$), Mm00514478_m1; nitric oxide synthase 2 (NOS2), Mm00440502_m1; integrin subunit alpha M (ITGAM), Mm00434455_m1; CD68, Mm03047340_m1; TNFα, Mm00443258_m1; IL-1β, Mm01336189_m1; chemokine (C-C motif) ligand 2 (CCL2), Mm00441242_m1; chemokine (C-C motif) ligand 5 (CCL5), Mm01302427_m1; suppressor of cytokine signaling 1 (SOCS1), Mm00782550_m1; phosphatidylinositol-3-4-5-trisphosphate 5-phosphatase 1 (SHIP-1), Mm00494987_m1; and GAPDH, Mm99999915_g1; Applied Biosystems, Carlsbad, CA] on an ABI 7900 HT FAST Real-Time PCR machine (Applied Biosystems). Samples were assayed in duplicate in 1 run (40 cycles), which was composed of 3 stages, 50 °C for 2 min, 95 °C for 10 s for each cycle (denaturation), and finally, the transcription step at 60 °C for 1 min. Gene expression was normalized by GAPDH and compared to the control sample to determine relative expression values by the $2^{-\Delta\Delta Ct}$ method.

miR Expression

A total of 10 ng of total RNA was reverse transcribed using TaqMan miRNA Reverse Transcription Kit (Applied Biosystems) with miRNA-specific primers. Reverse transcription reaction products (2 μl) were used for real-time PCR as described above. The following TaqMan miR expression assays were used: miR-155-5p (002571) and endogenous control U6 small nuclear RNA (snRNA) (001973) (Applied Biosystems). miR-155 expression was normalized by U6 snRNA and compared to the control sample to determine relative expression values by the $2^{-\Delta\Delta Ct}$ method.

Western Blot Analysis

Proteins from the ipsilateral cortical tissue were extracted using RIPA buffer and were equalized and loaded onto 5–20% gradient gels for SDS PAGE (Bio-Rad; Hercules, CA) as previously described [25]. Proteins were transferred onto nitrocellulose membranes and then blocked for 1 h in 5% milk in 1× TBS containing 0.05% Tween 20 (TBS-T) at room temperature. The membrane was incubated in mouse anti-SOCS1 (1:500; BD Thermo Fisher, Waltham, MA), mouse anti-SHIP-1 (1:1000; CST, Danvers, MA), or mouse anti-β-actin (1:5000; Sigma-Aldrich) overnight at 4 °C, then washed 3 times in TBS-T, and incubated in appropriate HRP-conjugated secondary antibodies (Jackson ImmunoResearch Laboratories, West Grove, PA) for 2 h at room temperature. Membranes were washed 3 times in TBS-T, and proteins were visualized using SuperSignal West Dura Extended Duration Substrate (Thermo Scientific, Rockford, IL). Chemiluminescence was captured ChemiDoc XRS+ System (Bio-Rad), and protein bands were quantified by densitometric analysis using Bio-Rad Molecular Imaging software. The data presented reflects the intensity of target protein band normalized based on the intensity of the endogenous control for each sample (expressed in arbitrary units).

Immunofluorescence Imaging

Twenty-micrometer coronal brain sections from sham and CCI mice at ~− 1.70 mm from the bregma were selected, and standard immunostaining techniques were employed. Briefly, 20-μm brain sections were washed 3 times with 1× PBS, blocked for 1 h in goat serum containing 0.4% Triton X-100, and incubated overnight at 4 °C with a combination of primary antibodies, including mouse anti-$gp91^{phox}$ (NOX2, 1:1000; BD Biosciences) and rat anti-CD68 (1:1000; AbD Serotec, Inc., Raleigh, NC). Sections were washed 3 times with 1× PBS and incubated with appropriate Alexa Fluor-conjugated secondary antibodies (Life Technologies) for 2 h at room temperature. Sections were washed 3 times with 1× PBS, counterstained with 4′,6-diamidino-2-phenylindole (DAPI) (1 μg/ml; Sigma, Dorset, UK), and mounted with glass coverslips using hydromount solution (National Diagnostics, Atlanta, GA). Images were acquired using a fluorescent Nikon Ti-E inverted microscope (Nikon Instrument, Inc., Melville, NY), at 10× (Plan Apo 10× NA 0.45) or 20× (Plan APO 20× NA 0.75) magnification. Exposure times were kept constant for all sections in each experiment. All images were quantified using Nikon ND-Elements software (AR 4.20.01). Colocalization of NOX2 and CD68 in microglia/macrophage was performed by binary operation intersection followed by thresholding. Twelve positive regions of interest near the lesion site per mouse were quantified (with $n = 5$ mice/group) and expressed as $NOX2^+/CD68^+$ cells/mm^2.

Stereology

Lesion Volume

Sixty-micrometer coronal sections from mice were stained with cresyl violet (FD NeuroTechnologies, Baltimore, MD), dehydrated, and mounted for analysis ($n = 9$/group). Lesion volume was quantified based on the Cavalieri method of unbiased stereology using Stereo Investigator software (MBF Biosciences, Williston, VT) as previously described [26]. Briefly, the lesion volume was quantified by outlining the missing tissue on the injured hemisphere using the Cavalieri estimator with a grid spacing of 0.1 mm. Every 8th section from a total of 96 sections was analyzed beginning from a random start point.

Neuronal Cell Loss

Cresyl violet-stained 60-μm coronal sections were used to quantify neuronal densities in the dentate gyrus region of the hippocampus of both sham and CCI mice. The optical fractionator method of stereology was employed as previously described [24]. Briefly, every 4th 60-μm section between − 1.22 and − 2.54 mm from the bregma was analyzed beginning from a random start point. A total of 5 sections were analyzed. The optical dissector had a size of 50 × 50 μm in the *x*-axis and the *y*-axis, respectively, with a height of 10 μm and a guard zone of 4 μm from the top of the section. The sampled regions of the dentate gyrus were demarcated in the injured hemisphere, and cresyl violet-positive cells were counted using Stereo Investigator software (MBF Biosciences). The volume of the dentate gyrus was measured using the Cavalieri estimator method with a grid spacing of 50 μm. The number of surviving neurons in each field was divided by the volume of the region of interest to obtain the cellular density expressed in counts/cubic millimeter.

Neurobehavioral Testing

Beam Walk

Motor function recovery was assessed using a beam walk test as previously described [27]. The beam walk test discriminates fine motor coordination differences between sham and CCI mice. The test consists of a narrow wooden beam (5 mm wide and 120 mm in length), which is suspended 300 mm above a tabletop. Mice were placed on 1 end of the beam, and the number of foot faults of the right hind limb was recorded over 50 steps. Mice were trained on the beam walk for 3 days prior to CCI and tested through 28 days post-injury.

Y-Maze Spontaneous Alternation

The Y-maze test assesses spatial working memory and was performed as previously described [23]. Briefly, the Y-maze (Stoelting Co., Wood Dale, IL) consisted of 3 identical arms, each arm 35 cm long, 5 cm wide, and 10 cm high, at an angle of 120° with respect to the other arms. One arm was randomly selected as the "start" arm, and the mouse was placed within and allowed to explore the maze freely for 5 min. Arm entries (arms A–C) were recorded by analyzing mouse activity using ANY-maze software (Stoelting Co., Wood Dale, IL). An arm entry was attributed when all 4 paws of the mouse entered the arm, and an alternation was designated when the mouse entered 3 different arms consecutively. The percentage of alternation was calculated as follows: total alternations × 100 / (total arm entries − 2). If a mouse scored > 50% alternations (the chance level for choosing the unfamiliar arm), this was indicative of spatial working memory.

Statistical Analysis

Randomization and blinding was performed as follows: a) individual who administered drugs was blinded to treatment group, and b) behavioral and stereological analyses were performed by individuals blinded to injury or treatment groups. Quantitative data were expressed as mean + standard error of the mean (SEM). Normality testing was performed and data sets passed normality (D'Agostino and Pearson omnibus normality test), and therefore, parametric statistical analysis was performed. Beam walk was analyzed by one-way repeated measures ANOVA to determine the interactions of time and groups, followed by *post hoc* adjustments using a Bonferroni's multiple comparison test. Y-maze and qRT-PCR were analyzed by one-way ANOVA, followed by *post hoc* adjustments using a Bonferroni's multiple comparison test. Stereological data were analyzed using a Student's *t* test (lesion volume) or one-way ANOVA (neuronal cell loss), followed by *post hoc* adjustments using the Student–Newman–Keuls test. Statistical analyses were performed using GraphPad Prism program, version 3.02 for Windows (GraphPad Software, San Diego, CA, USA). A p value < 0.05 was considered statistically significant.

Results

TBI Increases miR-155 Expression in Microglia/Macrophages in the Injured Cortex and Results in a Pro-inflammatory Activation Response

We induced moderate-level CCI in adult male C57Bl/6J mice and collected ipsilateral cortical tissue at 1 h, 24 h, 72 h, and

7 days post-injury for miR-155 expression analysis. When compared to sham control levels, there was a significant increase in miR-155 expression starting at 24 h post-injury ($p < 0.001$; Fig. 1a) that persisted through 7 days post-injury ($p < 0.001$ *vs* sham). We next isolated microglia/macrophages from the sham and injured cortex at 7 days post-injury using anti-CD11b MicroBeads and MACS technology [24]. miR-155 expression levels were robustly increased in enriched microglia/macrophages from the ipsilateral cortex when compared to sham-injured controls (> 5-fold increase; $p < 0.01$ *vs* sham; Fig. 1b). Furthermore, isolated microglia/macrophages had a pro-inflammatory phenotype, with significantly increased expression of CD68 ($p < 0.001$), IL-1β ($p < 0.001$), CCL5 ($p < 0.001$), and $p22^{phox}$ ($p < 0.01$) mRNA when compared to isolated microglia/macrophages from sham controls (Fig. 1b). Other pro-inflammatory markers (TNFα, NOX2) were also increased in microglia/macrophages from the injured cortex but failed to reach statistical significance (data not shown).

Acute ICV Administration of miR-155 Antagomir Attenuates TBI-Induced Pro-inflammatory Gene Expression in the Cortex

Next, moderate-level CCI mice were administered miR-155 antagomir (0.5 nmol) or equal concentration of negative control antagomir by single ICV injection in the ipsilateral lateral ventricle at 15 min post-injury, and cortical tissue was isolated at 24 h post-injury for analysis of miR-155, its direct targets, and pro-inflammatory cytokines. As predicted, there was a significant increase in miR-155 expression in the ipsilateral cortex at 24 h post-injury ($p < 0.05$ *vs* sham; Fig. 2a). Notably, when TBI mice were administered miR-155 antagomir, there was a significant decrease in cortical miR-155 expression when compared to TBI mice that received negative control antagomir treatment ($p < 0.05$; Fig. 2a). In addition, acute ICV administration of miR-155 antagomir also significantly reduced TBI-induced expression of IL-1β in the injured cortex ($p < 0.05$ *vs* TBI + neg control antagomir; Fig. 2a) and reduced TNFα expression, albeit nonsignificantly. We next assessed levels of known miR-155 direct targets, SOCS1 [28] and SHIP-1 [29], in the sham and injured cortex. TBI resulted in a significant reduction in SOCS1 mRNA and protein levels in the injured cortex at 24 h post-injury [$p < 0.05$ (mRNA) and $p < 0.001$ (protein) *vs* sham; Fig. 2b]. TBI mice that received miR-155 antagomir treatment had elevated SOCS1 mRNA levels at 24 h post-injury compared to the negative control antagomir-treated TBI group, but these failed to reach statistical significance. Furthermore, neither injury nor miR-155 antagomir treatment altered predicted target SHIP-1 mRNA or protein levels at 24 h post-injury (Fig. 2b).

Acute ICV Administration of miR-155 Antagomir Attenuates TBI-Induced Pro-inflammatory Gene Expression in the Hippocampus and Improves Cognitive Function Recovery in Injured Mice

In a follow-up study, moderate-level CCI mice were administered miR-155 antagomir (0.5 nmol) or equal concentration of

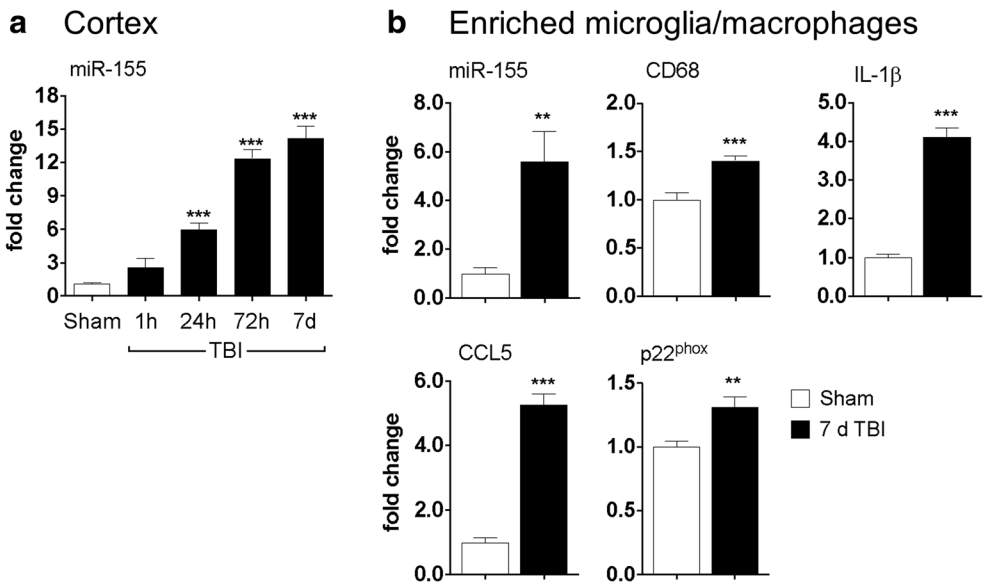

Fig. 1 TBI increases inflammatory miR-155 and neuroinflammatory gene expression in the cortex and in enriched microglia/macrophages. miR-155 expression is significantly increased in the injured cortex starting at 24 h post-injury and continued to increase through 7 days post-injury (A). Isolated microglia/macrophages from the injured cortex at 7 days post-injury displayed increased expression of miR-155 and upregulated pro-inflammatory gene expression, including CD68, IL-1β, CCL5, and $p22^{phox}$ (B). ***$p < 0.001$, **$p < 0.01$ *vs* sham. Data expressed as mean + SEM. One-way ANOVA, with Bonferroni *post hoc* adjustment in (A) and Student's *t* test in (B). $N = 5–6$/group

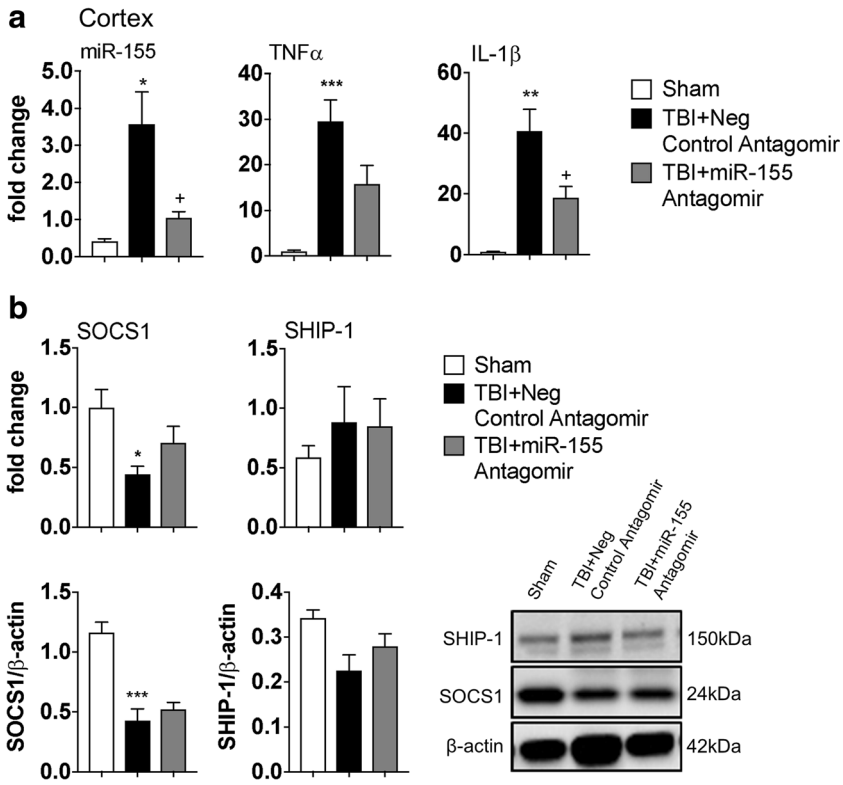

Fig. 2 Acute inhibition of miR-155 reduces TBI-induced pro-inflammatory gene expression in the cortex and alters expression of miR-155 direct targets. Acute ICV administration of miR-155 antagomir, beginning at 15 min post-injury, attenuated TBI-induced increases in miR-155, IL-1β, and TNFα expression in the injured cortex at 24 h post-injury (A). TBI decreased mRNA and protein levels of SOCS1, but not SHIP-1, in the injured cortex at 24 h post-injury. miR-155 antagomir treatment increased levels of SOCS1 mRNA similar to sham control levels (B). ***$p < 0.001$, **p<0.01, *$p < 0.05$ *vs* sham; $^{+}p < 0.05$ *vs* TBI + neg control antagomir-treated. Data expressed as mean + SEM. One-way ANOVA, with Bonferroni *post hoc* adjustment. $N = 5–6$/group

negative control antagomir by single ICV injection in the ipsilateral lateral ventricle at 15 min post-injury, and animals underwent cognitive testing at 7 days post-injury prior to tissue isolation for mRNA analysis. When we assessed hippocampus-dependent spatial working memory using the Y-maze test, sham mice showed 80.4 ± 4.4% spontaneous alteration, indicative of functional working memory. TBI resulted in a significant decrease in spontaneous alternation (60.3 ± 5.2%) in TBI mice treated with negative control antagomir ($p < 0.05$ *vs* sham; Fig. 3a). Notably, acute central administration of miR-155 antagomir in TBI mice reduced injury-induced deficits in cognitive function ($p < 0.5$ *vs* TBI + neg control antagomir), such that miR-155 antagomir-treated TBI mice had similar spontaneous alternation activity as sham mice. The total arm entries for each group of mice were identical in this test. We next assessed hippocampal expression of genes associated with microglial/macrophage activation and pro-inflammatory neuroinflammatory responses, including ITGAM, CD68, NOS2, $p22^{phox}$, NOX2, and TNFα. TBI resulted in significantly increased neuroinflammatory gene expression in TBI mice treated with negative control antagomir when compared to sham levels ($p < 0.05$, $p < 0.001$ *vs* sham; Fig. 3b). miR-155 antagomir treatment significantly decreased TBI-induced expression of ITGAM ($p < 0.001$), NOS2 ($p < 0.01$), NOX2 ($p < 0.001$), and $p22^{phox}$ ($p < 0.001$ *vs* TBI + neg control antagomir), whereas there was a nonsignificant reduction in TNFα expression.

Delayed ICV Administration of miR-155 Antagomir Starting at 24 h Post-injury Attenuates Post-traumatic Neuroinflammatory Responses at 7 Days Post-injury

We next investigated whether a delayed and more clinically relevant treatment paradigm could be effective in ameliorating neuroinflammatory responses following TBI. Moderate-level CCI mice received a continual infusion of a miR-155 antagomir (0.5 nmol/day) or equal concentration of negative control antagomir via contralateral ICV administration using ALZET pumps, beginning at 24 h post-injury and continuing through 7 days post-injury. Administration of the miR-155 antagomir significantly decreased TBI-induced upregulation of miR-155 in the hippocampus at 7 days post-injury ($p < 0.05$ *vs* TBI + neg control antagomir; Fig. 4). Furthermore, miR-155 antagomir treatment reduced expression of pro-inflammatory and microglial/macrophage activation genes in the hippocampus, including ITGAM ($p < 0.05$), CD68 ($p < 0.05$), NOX2 ($p < 0.05$), $p22^{phox}$ ($p < 0.05$), TNFα ($p < 0.05$), and CCL2 ($p < 0.05$ *vs* TBI + neg control antagomir; Fig. 4). There was a reduction in IL-1β and CCL5 expression with delayed miR-155 antagomir treatment; however, these changes failed to reach statistical significance.

It is important to note that while there were significant TBI-induced increases in miR-155 and pro-inflammatory gene expression in the ipsilateral cortex of negative control antagomir-treated TBI mice at 7 days post-injury, these pro-inflammatory markers were not attenuated by miR-155

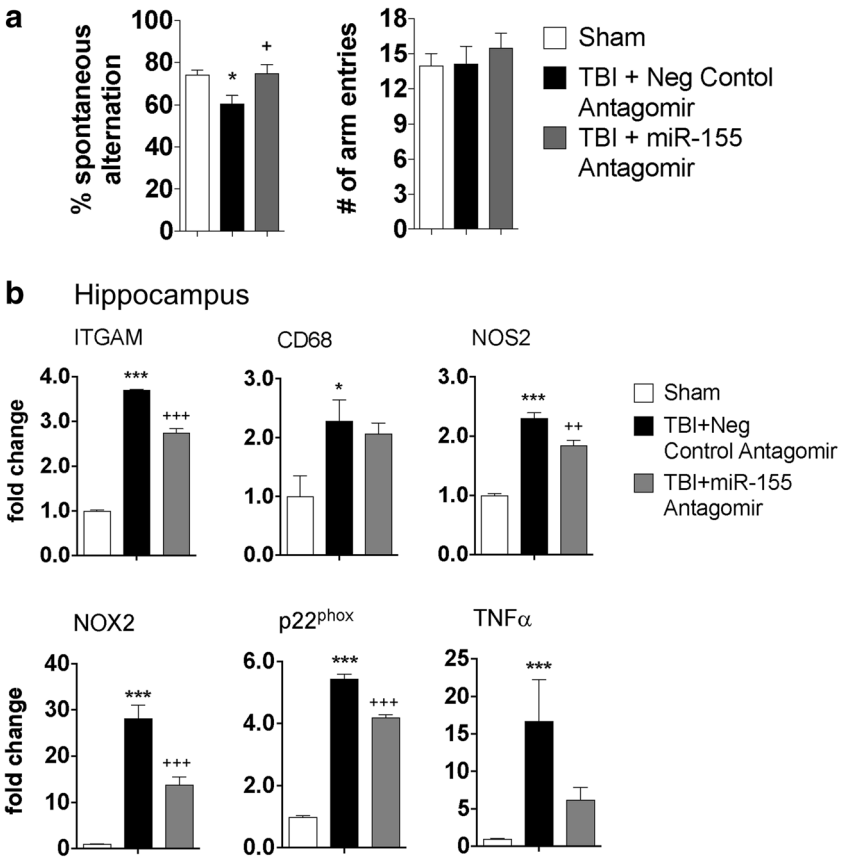

Fig. 3 Acute inhibition of miR-155 attenuates TBI-induced impairments in cognitive function and reduces pro-inflammatory gene expression in the injured hippocampus. Acute ICV administration of miR-155 antagomir, beginning at 15 min post-injury, significantly reduced deficits in cognitive function at 7 days post-injury using the Y-maze test (A). In addition, acute ICV administration of miR-155 antagomir significantly reduced expression of pro-inflammatory markers including ITGAM, CD68, NOS2, $p22^{phox}$, and NOX2, but not TNFα, in the ipsilateral hippocampus at 7 days post-injury. $^{***}p < 0.001$, $^{*}p < 0.05$ *vs* sham; $^{+++}p < 0.001$, $^{++}p<0.01$, $^{+}p < 0.05$ *vs* TBI + neg control antagomir-treated. Data expressed as mean + SEM. One-way ANOVA, with Bonferroni *post hoc* adjustment. $N = 8$/group

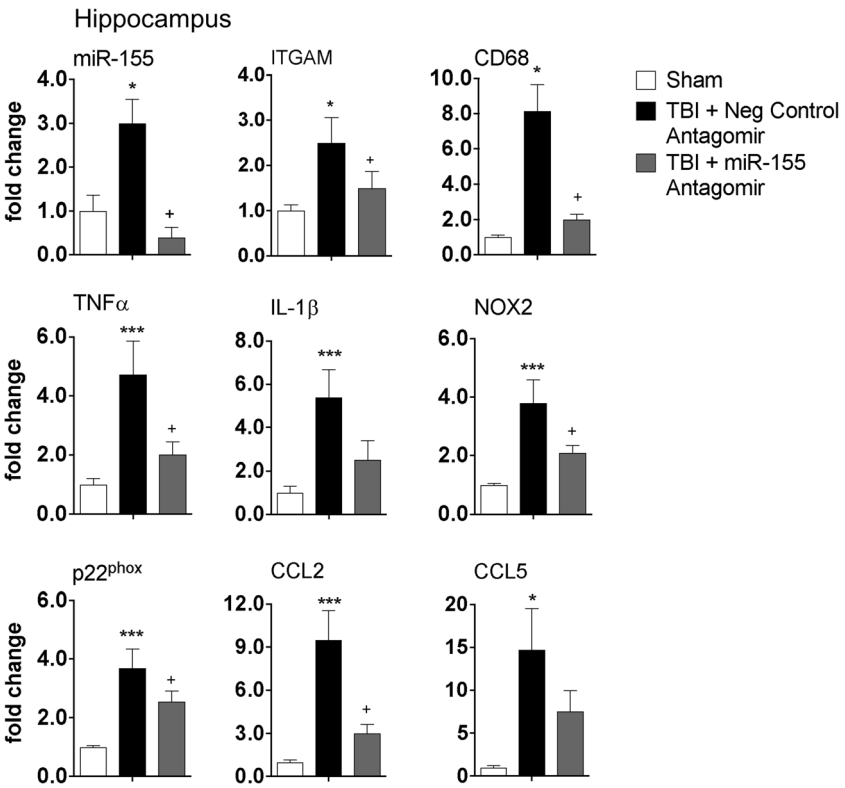

Fig. 4 Delayed inhibition of miR-155 reduces hippocampal miR-155 and pro-inflammatory gene expression at 7 days post-injury. Delayed and continual ICV administration of miR-155 antagomir, beginning at 24 h post-injury, significantly reduced miR-155 expression in the injured hippocampus at 7 days post-injury. TBI-induced expression of pro-inflammatory and microglial activation genes, ITGAM, CD68, NOX2, $p22^{phox}$, TNFα, and CCL2, was significantly reduced with treatment. Hippocampal IL-1β and CCL5 expression was also reduced in the TBI + miR-155 antagomir-treated group but failed to reach statistical significance when compared to the TBI + neg control antagomir-treated group. $^{***}p < 0.001$, $^{*}p < 0.05$ *vs* sham; $^{+}p < 0.05$ *vs* TBI + neg control antagomir-treated. Data expressed as mean + SEM. One-way ANOVA, with Bonferroni *post hoc* adjustment

antagomir treatment (Table 1). Furthermore, miR-155 antagomir treatment did not alter TBI-induced expression of miR-155 direct targets, SHIP-1 or SOCS1, in the ipsilateral cortex at 7 days post-injury (Table 1).

Delayed ICV Administration of miR-155 Antagomir Improves Long-Term Motor But Not Cognitive Function After TBI

To determine whether miR-155 inhibition could improve neurological function following TBI, we repeated the delayed and continuous miR-155 antagomir infusion protocol in a separate cohort of CCI mice and followed animals for 28 days post-injury. We assessed motor and cognitive function recovery using beam walk and Y-maze behavioral tests, respectively. First, we performed beam walk to assess deficits in fine motor coordination. When compared to sham mice, TBI resulted in significant motor function impairments in negative control antagomir-treated TBI mice, with 50 ± 0 foot faults (FFs; mean ± SEM) at 1 day post-injury and persistent foot faults through 28 days post-injury (39 ± 6 FFs; $p < 0.001$ *vs* sham; Fig. 5a). Delayed administration of miR-155 antagomir significantly improved motor function recovery after TBI, with miR-155 antagomir-treated mice having 30 ± 3 and 29 ± 3 foot faults at 14 days and 21 days post-injury, respectively ($p < 0.05$ *vs* TBI + neg control antagomir). We then assessed hippocampus-dependent spatial working memory using the Y-maze test. When compared to % spontaneous alternation in sham mice (74.0 ± 4.5%), TBI significantly decreased spontaneous alternations (65.6 ± 2.9%) in TBI mice treated with negative control antagomir ($p < 0.05$ *vs* sham; Fig. 5b). Delayed administration of the miR-155 antagomir failed to improve spatial working memory in this test, and miR-155 antagomir-treated TBI mice had equivalent spontaneous alternation activity (60.7 ± 3.9%) as negative control antagomir-treated TBI mice.

Delayed ICV Administration of miR-155 Antagomir Reduces TBI-Induced Cortical Lesion Volume and the Number of Reactive Microglia/Macrophages in the Injured Cortex

Next, we quantified TBI-induced lesion volume in the ipsilateral cortex of miR-155 antagomir and negative control antagomir-treated TBI mice at 28 days post-injury. The lesion volume of negative control antagomir-treated TBI mice was 8.62 ± 1.10 mm^3 (Fig. 6a). Notably, the delayed miR-155 antagomir treatment significantly reduced the lesion to 6.56 ± 0.73 mm^3 ($p < 0.05$ *vs* TBI + neg control antagomir). TBI in negative control antagomir-treated TBI mice also resulted in significant neuronal loss in the dentate gyrus when compared to sham levels ($p < 0.05$ *vs* sham; Fig. 6b). However, delayed miR-155 antagomir treatment failed to rescue TBI-induced neuronal loss in the dentate gyrus.

We finally evaluated NOX2 expression in reactive microglia/macrophages that coexpressed CD68, a marker of highly phagocytic activity, in the injured cortex. TBI induced robust NOX2 expression in $CD68^+$ cells that displayed amoeboid morphological features in the cortex of negative control antagomir-treated TBI mice (Fig. 7a, b). Notably, delayed administration of miR-155 antagomir significantly reduced the number of $NOX2^+/CD68^+$ microglia/macrophages in the injured cortex ($p < 0.05$ *vs* TBI + neg control antagomir).

Discussion

We have previously shown that sustained microglial activation after brain trauma contributes to subsequent progressive neurodegeneration and associated neurological deficits [21–25]. Consistent with recent findings [30], we demonstrate that miR-155 rapidly and progressively increases in the ipsilateral cortex through 7 days post-injury. In an earlier study, we demonstrated increased post-traumatic expression of miR-

Table 1 Delayed inhibition of miR-155 does not alter miR-155, direct target, or pro-inflammatory gene expression in the injured cortex at 7 days post-injury. Delayed and continual ICV infusion of miR-155 antagomir, beginning at 24 h post-injury, does not alter expression of miR-155, its direct targets (SOCS1 and SHIP-1), or pro-inflammatory genes (NOX2, $p22^{phox}$, TNFα, or IL-1β) in the injured cortex at 7 days post-injury

	Ipsilateral cortical miR and mRNA expression ($2^{-\Delta\Delta Ct}$; fold change)		
	Sham	TBI + neg control antagomir	TBI + miR-155 antagomir
miR-155	1.00 ± 0.17	10.94 ± 2.42	10.79 ± 2.93
SHIP-1	1.00 ± 0.06	2.61 ± 0.31**	2.89 ± 0.31
SOCS1	1.00 ± 0.07	1.58 ± 0.20*	1.81 ± 0.16
NOX2	1.00 ± 0.08	9.71 ± 3.19*	16.92 ± 2.78
$p22^{phox}$	1.00 ± 0.08	5.68 ± 1.24**	6.32 ± 0.67
TNFα	1.00 ± 0.12	9.49 ± 2.55*	11.94 ± 1.67
IL-1β	1.00 ± 0.09	9.47 ± 4.07	7.28 ± 1.26

Data are expressed as mean + SEM (one-way ANOVA, with Bonferroni *post hoc* adjustment). $N = 6–7$/group
*$p < 0.05$; **$p < 0.01$ *vs* sham counterparts

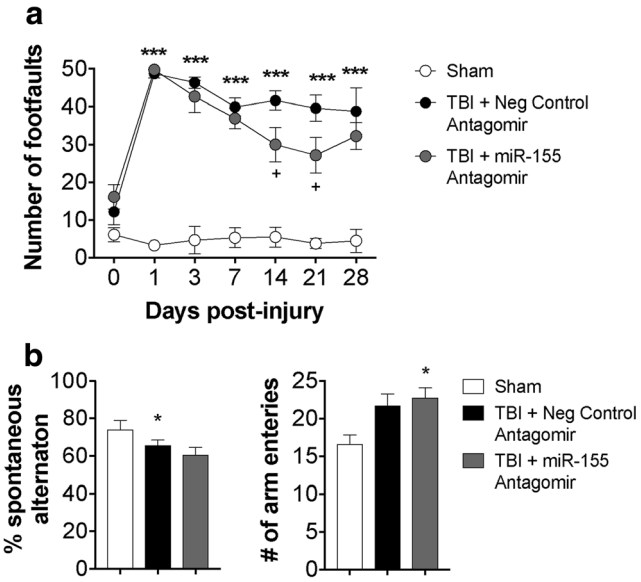

Fig. 5 Delayed inhibition of miR-155 improves fine motor coordination, but not cognitive function following TBI. Delayed and continual ICV infusion of miR-155 antagomir, beginning at 24 h post-injury, significantly reduced the number of TBI-induced foot faults on the beam walk test at 14 days and 21 days post-injury (A). However, this delayed treatment regime did not ameliorate TBI-induced cognitive deficits in the Y-maze test at 11 days post-injury (B). $^{*}p < 0.05$, $^{***}p < 0.001$ *vs* sham; $^{+}p < 0.05$ *vs* TBI + neg control antagomir-treated. Data expressed as mean + SEM. Repeated measures one-way ANOVA with Bonferroni *post hoc* adjustment in (A). One-way ANOVA with Bonferroni *post hoc* adjustment in (B). $N = 12–15$/group

155 in the injured cortex at 24 h that was associated with elevated expression of several pro-inflammatory genes (NOS2, TNFα, IL-1β, IL-6, and CCL2) [19]. Here, we confirmed that microglia/macrophages isolated from the injured cortex show increased miR-155 expression that was associated with elevations in markers of microglial/macrophage activation and pro-inflammatory signaling—including IL-1β, TNFα, CCL5, and NADPH oxidase subunits (NOX2, $p22^{phox}$). The expression level of ROS-producing NOX2 is highly elevated in reactive microglia/macrophages ($NOX2^{+}$/$TNF\alpha^{+}$/$CD68^{+}$) in the injured cortex at the peak of neuroinflammation in this model (7 days post-injury) and remains elevated for several months [22, 23, 31]. Similar to the observed therapeutic effects in the current study, pharmacological inhibition of NOX2 starting at 24 h post-injury shifts microglia/macrophages towards an anti-inflammatory phenotype, which is associated with reduced oxidative damage in neurons and improved neurological recovery [23, 24].

miR-155 is a critical regulator of Toll-like receptor (TLR) 3 and 4 and interferon (IFN)-γ-mediated signaling in macrophages [32–35]. In addition, macrophages from miR-155 knockout or from wild-type mice treated with a miR-155 oligonucleotide inhibitor show decreased expression of pro-inflammatory markers including NOX2, TNFα, and IL-1β [32]. miR-155 is also robustly upregulated in activated microglia and promotes a pro-inflammatory phenotype [5, 36]. Notably, miR-155 knockout microglia or anti-miR-155 oligonucleotides reduce nitric oxide and pro-inflammatory cytokines in response to lipopolysaccharide stimulation (TLR4 ligand), as well as suppress microglial cell-mediated neurotoxicity in coculture model systems [6]. In the present study, we demonstrate that inhibiting miR-155 in the early post-traumatic period, using single-dose ICV administration of miR-155 antagomir, decreases microglial/macrophage activation and pro-inflammatory signaling in the injured cortex and hippocampus at 1 day and 7 days post-injury, respectively. This attenuation of the post-traumatic neuroinflammatory response was associated with reduced impairments in spatial working memory.

In order to minimize toxicity, we administered the miR-155 antagomir (inhibitory oligonucleotides) *in vivo* without additional transfection reagents [37]. Although prior reports, such as those by Reschke et al. [38], used modifications of the oligonucleotides (e.g., cholesterol) to improve their ability to penetrate cellular membranes without additional transfection reagents, other studies suggest that the range of miR-targeting oligonucleotides that can independently penetrate membranes may be larger than previously thought. For example, Morris et al. [39] used phosphorothioate (PS)-modified backbones (Power Inhibitors) without transfection reagents to silence their target miRs in the brain following intracerebroventricular injection. Moreover, Stein et al. [37] describe the process of unassisted "naked" delivery of oligonucleotides, coining the term "gymnosis"; although these authors focused their studies on PS-containing oligonucleotides, they note that additional modification may also contribute to gymnosis, including 2′-*O*-methyl modifications. The Dharmacon-produced oligonucleotides that were used in our TBI studies include 2′-*O*-methyl modifications, as detailed in a prior publication linked to their patent [40]. Other studies have reported on gymnosis in modulating miRs; 2′-*O*-methyl modifications, such as an oligonucleotide produced by Dharmacon, showed miR inhibitory activity in the absence of transfection reagents [41]. Although the mechanisms underpinning gymnosis have yet to be fully elucidated, we believe that this process may account, at least in part, for the ability of the miR-155 oligonucleotides used in our studies to penetrate the cellular membrane and target intracellular signaling in the absence of transfection reagents. Another possible mechanism that may increase membrane permeability for therapeutic delivery of miR antagomirs involves post-traumatic mechanoporation [42–44].

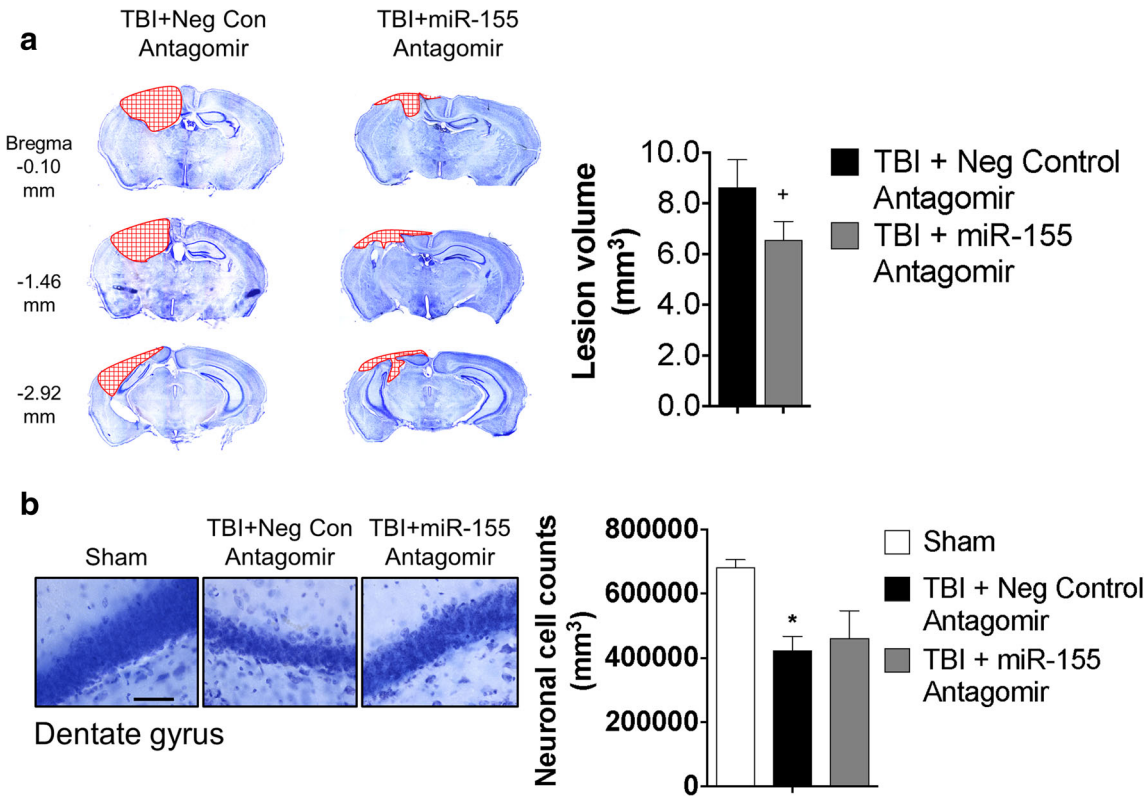

Fig. 6 Delayed inhibition of miR-155 decreases lesion volume but does not prevent neuronal loss in the hippocampus following TBI. Representative images from lesion of TBI + neg control antagomir and TBI + miR-155 antagomir at 28 days post-injury. Delayed and continual ICV infusion of miR-155 antagomir, beginning at 24 h post-injury, significantly decreased lesion volume (A). Representative images of the dentate gyrus of sham, TBI + neg control antagomir, and TBI + miR-155 antagomir at 28 days post-injury. Bar = 50 μm. Delayed inhibition of miR-155 did not prevent neuronal loss in the dentate gyrus when compared to the TBI + neg control antagomir-treated group at 28 days post-injury (B). $^{*}p < 0.05$ *vs* sham; $^{+}p < 0.05$ *vs* TBI + neg control antagomir-treated. Data expressed as mean + SEM. Student's *t* test in (A). One-way ANOVA with Bonferroni *post hoc* adjustment in (B). $N = 8$/group

A challenge for developing translational neuroprotective treatment strategies in TBI is identifying targets for pharmacological intervention that have a long therapeutic window [45]. Chronic microglial activation and molecular mechanisms underlying secondary neuroinflammation are recognized as potential therapeutic targets for severe TBI [46]. Therefore, to test a more clinically relevant treatment paradigm, we evaluated delayed administration of the miR-155 antagomir, starting at 24 h post-injury and continuing for 6 days. Such treatment significantly reduced miR-155 levels in the injured hippocampus at 7 days and attenuated TBI-induced increased expression of markers of microglial/macrophage activation and pro-inflammatory signaling. Inhibition of miR-155 also decreased TBI-induced chemokine expression, including CCL2. Morganti and colleagues [47] recently demonstrated that inhibition of CCL2–CCR2 signaling following TBI, using a selective CCR2 antagonist, attenuated pro-inflammatory signaling. These effects were associated with improved hippocampus-dependent learning and memory at 28 days post-injury [47]. CCR2 knockout mice also show reduced lesion volume and decreased neuroinflammation at 3 days following severe CCI [48]. CCL5 is robustly upregulated acutely after TBI in mice [49] and humans [50]; elevated levels of CCL5 in plasma of TBI patients at admission correlate with poor outcome [51]. Here, we demonstrated that moderate-level TBI increases CCL2 and CCL5 expression at 7 days post-injury, and that delayed inhibition of miR-155 attenuates both CCL2 and CCL5 levels. Notably, leukocyte-specific deletion of miR-155 reduces the expression of CCL2 in pro-inflammatory macrophages, which results in recruitment of monocytes to clear atherosclerotic plaques and attenuate vascular inflammation in mouse models of atherosclerosis [52]. To our knowledge, this is the first study linking miR-155 and chemokine signaling (CCL2/CCL5) in the context of macrophage/microglial activation after experimental TBI.

Delayed miR-155 antagomir treatment also improved fine motor coordination in TBI mice at 14 days and 21 days, but not at 28 days. The absence of significant effects at the latter time point may reflect washout of miR-155 antagomir from the CNS over time. Furthermore, unlike the acute miR-155 treatment paradigm, delayed inhibition of miR-155 failed to reduce TBI-induced impairments of hippocampus-dependent working memory in the Y-maze test and did not reduce

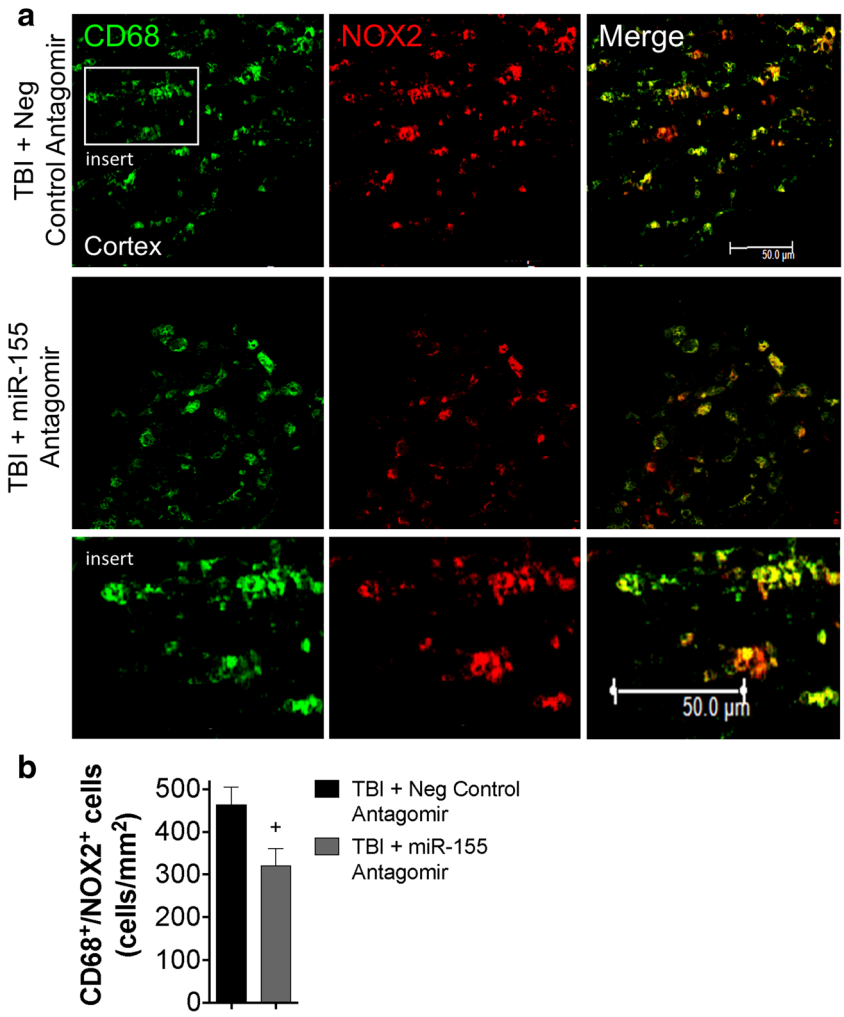

Fig. 7 Delayed inhibition of miR-155 decreases NOX2 expression in reactive microglia/macrophages in the injured cortex at 28 days post-injury. Representative images from the cortex of TBI + neg control antagomir and TBI + miR-155 antagomir at 28 days post-injury. Bar = 50 μm (A). Immunofluorescence analysis of NOX2 (red) and CD68 (green) demonstrates that delayed and continual ICV infusion of miR-155 antagomir, beginning at 24 h post-injury, significantly decreased NOX2 expression in reactive microglia/macrophages. $^{+}p < 0.05$ *vs* TBI + neg control antagomir-treated (B). Data expressed as mean + SEM. Student's *t* test in (A). $N = 5$/group

neuronal cell loss in the hippocampus (dentate gyrus). However, delayed inhibition of miR-155 significantly reduced cortical lesion volume at 28 days, as well as the number of highly reactive $NOX2^{+}/CD68^{+}$ microglia/macrophages in the injured cortex.

The miR-155-induced pro-inflammatory response has been linked, in part, to suppression of its predicted targets including SOCS1 [6, 13, 53] and SHIP-1 [13, 54]. SOCS1 is a negative regulator of IFN signaling and a validated target of miR-155 that functions to inhibit STAT1 [30], a key transcription factor for IFN signaling, whereas SHIP-1 helps control immune cell function by downregulating PI3K signaling pathways [55]. The links among miR-155 expression, SOCS-1 and SHIP-1 inhibition, and production of inflammatory mediators in myeloid cells suggest that the deregulation of miR-155 can drive progressive neuroinflammation by disturbing the protective function of SOCS1/SHIP-1, increasing pro-inflammatory cytokine and nitric oxide production [6, 13, 53, 54, 56]. TBI significantly reduced SOCS1, but not SHIP-1, in the injured cortex at 24 h post-injury. Treatment with the miR-155 antagomir attenuated the post-traumatic decrease of SOCS1, with mRNA levels not significantly different from sham control levels. However, SOCS1 protein levels did not differ between miR-155 antagomir and negative control antagomir treatment groups at 24 h. This time point may be too early to detect protein changes. Decreased SOCS1 mRNA expression has been reported in miR-155 knockout mice subjected to moderate-level CCI as compared to wild-type CCI mice [30]. However, the results in miR-155 knockout mice contrast with ours and those in experimental stroke, where miR-155 inhibitors administered to distal middle cerebral artery occlusion (dMCAO) mice upregulate SOCS1 and SHIP-1 in the injured cortex at 7 days post-injury, a time point that was associated with robust anti-inflammatory activity [13]. The effects of miR-155 inhibitors on SOCS1/SHIP-1 in the dMCAO model were lost at later time points (14 days post-injury), suggesting that dosing and duration of miR-155 antagomir treatment may be relevant for optimal neuroprotection in CNS injury models. Further translational studies, including dose-response and treatment duration, will be needed to optimize the anti-inflammatory and neuroprotective effects of miR-155 antagomir treatment after TBI.

Perhaps surprisingly, central administration of miR-155 antagomir attenuated TBI-induced miR-155 elevation in the injured cortex. However, this observation is consistent with prior work demonstrating that inhibitor-induced miR degradation can occur under certain conditions [57]. It is also possible that the miR-155 reduction observed in our TBI study reflects an indirect effect in which miR-155 inhibition/sequestration in an early cell subpopulation may reduce propagation of pro-inflammatory secondary injury responses that limit later miR-155 induction.

Our study revealed region-specific anti-inflammatory effects of miR-155 antagomir in the injured cortex and hippocampus. Possible reasons for region-specific responses may include site of injection for miR-155 antagomirs and/or increased sensitivity of the hippocampus to miR-155-based treatments. When we infused miR-155 antagomir into the contralateral ventricle using a 7-day mini-osmotic pump (inserted at 24 h post-injury) infusion, there were reduced miR-155 expression and decreases of various pro-inflammatory and microglial cell-related markers in the ipsilateral hippocampus at 7 days post-injury. However, the ipsilateral cortex of these mice did not show changes in the expression of miR-155 or pro-inflammatory markers. The anti-inflammatory effects in the hippocampus may reflect increased access of the miR-155 antagomir under these conditions, as this region is closer to the infusion site than the ipsilateral cortex tissue examined. An alternative explanation for site-specific effects may be that several miR-155 targets are highly expressed in the hippocampus [58, 59], thus possibly indicating that the hippocampus is more sensitive to modulation by miR-155. The fact that genetic ablation of miR-155 is associated with a decrease of inflammatory-mediated impairments in neurogenesis following systemic LPS challenge [59] may be consistent with the latter interpretation.

A recent study reported exacerbation of hippocampal neurodegeneration, as well as increased microglial/macrophage activation, in miR-155 knockout mice following CCI [30]. Such apparently divergent results may reflect cell-specific responses and/or compensatory effects due to use of a constitutive miR-155 knockout model. Thus, Harrison and colleagues [30] reported that miR-155 was upregulated in hippocampal neurons at 24 h post-injury. Further studies addressing cell-specific modulation of miR-155 using miR-155$^{fl/fl}$ transgenic models [60] will be needed to address this apparent discrepancy. Another potentially important issue is the role of miR-155 in mitochondrial dysfunction after CNS injury, given that administration of a miR-155 mimic can cause mitochondrial dysfunction in macrophages [61]. In addition, miR-155 has been reported to be markedly upregulated in isolated mitochondria from the hippocampus at 12 h post-injury [20]. Moreover, it was recently shown that pro-inflammatory cytokines increase miR-155 levels in the hippocampus after TBI, which suppressed peroxisome proliferator-activated receptor gamma coactivator 1-alpha (PGC-1α) mRNA, altering mitochondrial biogenesis and possibly mitochondrial respiratory dysfunction [62]. Given the rapid onset of mitochondrial dysfunction following TBI (within minutes), if miR-155 contributes to such deficits, this may help explain the apparently less effective therapeutic response to delayed treatment.

In summary, we demonstrate that moderate-to-severe TBI causes increased miR-155 expression in microglia/macrophages, and that selective miR-155 inhibition reduces post-traumatic neuroinflammatory responses and behavioral dysfunction. Thus, miR-155 should be considered as a potential therapeutic target in head injury.

Funding Information This work was supported by NIH R01 NS037313 (AIF), R01 NS082308 (DJL), and T32 AI095190 (SJD).

References

1. Griffiths-Jones, S., *miRBase: the microRNA sequence database*. Methods Mol Biol, 2006. **342**: p. 129–138.
2. Dickey, L.L., et al., *MicroRNA 155 and viral-induced neuroinflammation*. J Neuroimmunol, 2017. **308**: p. 17–24.
3. Ponomarev, E.D., T. Veremeyko, and H.L. Weiner, *MicroRNAs are universal regulators of differentiation, activation, and polarization of microglia and macrophages in normal and diseased CNS*. Glia, 2013. **61**(1): p. 91–103.
4. Quinn, S.R. and L.A. O'Neill, *A trio of microRNAs that control Toll-like receptor signalling*. Int Immunol, 2011. **23**(7): p. 421–425.
5. Freilich, R.W., M.E. Woodbury, and T. Ikezu, *Integrated expression profiles of mRNA and miRNA in polarized primary murine microglia*. PLoS One, 2013. **8**(11): p. e79416.
6. Cardoso, A.L., et al., *miR-155 modulates microglia-mediated immune response by down-regulating SOCS-1 and promoting cytokine and nitric oxide production*. Immunology, 2012. **135**(1): p. 73–88.
7. Al-Haidari, A.A., I. Syk, and H. Thorlacius, *MiR-155-5p positively regulates CCL17-induced colon cancer cell migration by targeting RhoA*. Oncotarget, 2017. **8**(9): p. 14887–14896.
8. Elmesmari, A., et al., *MicroRNA-155 regulates monocyte chemokine and chemokine receptor expression in Rheumatoid Arthritis*. Rheumatology (Oxford), 2016. **55**(11): p. 2056–2065.
9. Matsukura, S., et al., *Overexpression of microRNA-155 suppresses chemokine expression induced by Interleukin-13 in BEAS-2B human bronchial epithelial cells*. Allergol Int, 2016. **65 Suppl**: p. S17–S23.
10. Rajasekhar, M., et al., *MicroRNA-155 contributes to enhanced resistance to apoptosis in monocytes from patients with rheumatoid arthritis*. J Autoimmun, 2017. **79**: p. 53–62.
11. Lippai, D., et al., *Chronic alcohol-induced microRNA-155 contributes to neuroinflammation in a TLR4-dependent manner in mice*. PLoS One, 2013. **8**(8): p. e70945.
12. Gaudet, A.D., et al., *miR-155 Deletion in Mice Overcomes Neuron-Intrinsic and Neuron-Extrinsic Barriers to Spinal Cord Repair*. J Neurosci, 2016. **36**(32): p. 8516–8532.
13. Pena-Philippides, J.C., et al., *In vivo inhibition of miR-155 significantly alters post-stroke inflammatory response*. J Neuroinflammation, 2016. **13**(1): p. 287.

14. Tan, Y., et al., *Suppression of microRNA-155 attenuates neuropathic pain by regulating SOCS1 signalling pathway*. Neurochem Res, 2015. **40**(3): p. 550–560.
15. Murugaiyan, G., et al., *Silencing microRNA-155 ameliorates experimental autoimmune encephalomyelitis*. J Immunol, 2011. **187**(5): p. 2213–2221.
16. Koval, E.D., et al., *Method for widespread microRNA-155 inhibition prolongs survival in ALS-model mice*. Hum Mol Genet, 2013. **22**(20): p. 4127–4135.
17. Thome, A.D., et al., *microRNA-155 Regulates Alpha-Synuclein-Induced Inflammatory Responses in Models of Parkinson Disease*. J Neurosci, 2016. **36**(8): p. 2383–2390.
18. Caballero-Garrido, E., et al., *In Vivo Inhibition of miR-155 Promotes Recovery after Experimental Mouse Stroke*. J Neurosci, 2015. **35**(36): p. 12446–12464.
19. Kumar, A., et al., *Microglial-derived microparticles mediate neuroinflammation after traumatic brain injury*. J Neuroinflammation, 2017. **14**(1): p. 47.
20. Wang, W.X., et al., *Mitochondria-associated microRNAs in rat hippocampus following traumatic brain injury*. Exp Neurol, 2015. **265**: p. 84–93.
21. Kabadi, S.V., et al., *Selective CDK inhibitor limits neuroinflammation and progressive neurodegeneration after brain trauma*. J Cereb Blood Flow Metab, 2012. **32**(1): p. 137–149.
22. Loane, D.J., et al., *Progressive neurodegeneration after experimental brain trauma: association with chronic microglial activation*. J Neuropathol Exp Neurol, 2014. **73**(1): p. 14–29.
23. Kumar, A., et al., *NOX2 drives M1-like microglial/macrophage activation and neurodegeneration following experimental traumatic brain injury*. Brain Behav Immun, 2016. **58**: p. 291–309.
24. Kumar, A., et al., *Microglial/Macrophage Polarization Dynamics following Traumatic Brain Injury*. J Neurotrauma, 2016. **33**(19): p. 1732–1750.
25. Barrett, J.P., et al., *NOX2 deficiency alters macrophage phenotype through an IL-10/STAT3 dependent mechanism: implications for traumatic brain injury*. J Neuroinflammation, 2017. **14**(1): p. 65.
26. Kumar, A., et al., *Traumatic brain injury in aged animals increases lesion size and chronically alters microglial/macrophage classical and alternative activation states*. Neurobiol Aging, 2013. **34**(5): p. 1397–1411.
27. Loane, D.J., et al., *Amyloid precursor protein secretases as therapeutic targets for traumatic brain injury*. Nat Med, 2009. **15**(4): p. 377–379.
28. Wang, P., et al., *Inducible microRNA-155 feedback promotes type I IFN signaling in antiviral innate immunity by targeting suppressor of cytokine signaling 1*. J Immunol, 2010. **185**(10): p. 6226–6233.
29. O'Connell, R.M., et al., *Inositol phosphatase SHIP1 is a primary target of miR-155*. Proc Natl Acad Sci U S A, 2009. **106**(17): p. 7113–7118.
30. Harrison, E.B., et al., *Induction of miR-155 after Brain Injury Promotes Type 1 Interferon and has a Neuroprotective Effect*. Front Mol Neurosci, 2017. **10**: p. 228.
31. Byrnes, K.R., et al., *Delayed mGluR5 activation limits neuroinflammation and neurodegeneration after traumatic brain injury*. J Neuroinflammation, 2012. **9**: p. 43.
32. Jablonski, K.A., et al., *Control of the Inflammatory Macrophage Transcriptional Signature by miR-155*. PLoS One, 2016. **11**(7): p. e0159724.
33. McCoy, C.E., et al., *IL-10 inhibits miR-155 induction by toll-like receptors*. J Biol Chem, 2010. **285**(27): p. 20492–20498.
34. Sun, Y., et al., *miR-155 mediates suppressive effect of progesterone on TLR3, TLR4-triggered immune response*. Immunol Lett, 2012. **146**(1–2): p. 25–30.
35. Tili, E., et al., *Modulation of miR-155 and miR-125b levels following lipopolysaccharide/TNF-alpha stimulation and their possible roles in regulating the response to endotoxin shock*. J Immunol, 2007. **179**(8): p. 5082–5089.
36. Moore, C.S., et al., *miR-155 as a multiple sclerosis-relevant regulator of myeloid cell polarization*. Ann Neurol, 2013. **74**(5): p. 709–720.
37. Stein, C.A., et al., *Efficient gene silencing by delivery of locked nucleic acid antisense oligonucleotides, unassisted by transfection reagents*. Nucleic Acids Res, 2010. **38**(1): p. e3.
38. Reschke, C.R., et al., *Potent Anti-seizure Effects of Locked Nucleic Acid Antagomirs Targeting miR-134 in Multiple Mouse and Rat Models of Epilepsy*. Mol Ther Nucleic Acids, 2017. **6**: p. 45–56.
39. Morris, G., et al., *Spared CA1 pyramidal neuron function and hippocampal performance following antisense knockdown of microRNA-134*. Epilepsia, 2018. **59**(8): p. 1518–1526.
40. Vermeulen, A., et al., *Double-stranded regions are essential design components of potent inhibitors of RISC function*. RNA, 2007. **13**(5): p. 723–730.
41. Torres, A.G., R.N. Threlfall, and M.J. Gait, *Potent and sustained cellular inhibition of miR-122 by lysine-derivatized peptide nucleic acids (PNA) and phosphorothioate locked nucleic acid (LNA)/2'-O-methyl (OMe) mixmer anti-miRs in the absence of transfection agents*. Artif DNA PNA XNA, 2011. **2**(3): p. 71–78.
42. Farkas, O., J. Lifshitz, and J.T. Povlishock, *Mechanoporation induced by diffuse traumatic brain injury: an irreversible or reversible response to injury?* J Neurosci, 2006. **26**(12): p. 3130–3140.
43. LaPlaca, M.C., et al., *Mechanoporation is a potential indicator of tissue strain and subsequent degeneration following experimental traumatic brain injury*. Clin Biomech (Bristol, Avon), 2018.
44. Levine, J., et al., *Traumatically injured astrocytes release a proteomic signature modulated by STAT3-dependent cell survival*. Glia, 2016. **64**(5): p. 668–694.
45. Loane, D.J. and A.I. Faden, *Neuroprotection for traumatic brain injury: translational challenges and emerging therapeutic strategies*. Trends Pharmacol Sci, 2010. **31**(12): p. 596–604.
46. Simon, D.W., et al., *The far-reaching scope of neuroinflammation after traumatic brain injury*. Nat Rev Neurol, 2017. **13**(9): p. 572.
47. Morganti, J.M., et al., *CCR2 antagonism alters brain macrophage polarization and ameliorates cognitive dysfunction induced by traumatic brain injury*. J Neurosci, 2015. **35**(2): p. 748–760.
48. Israelsson, C., et al., *Interacting chemokine signals regulate dendritic cells in acute brain injury*. PLoS One, 2014. **9**(8): p. e104754.
49. Sandhir, R., et al., *Differential expression of cytokines and chemokines during secondary neuron death following brain injury in old and young mice*. Neurosci Lett, 2004. **369**(1): p. 28–32.
50. Stefini, R., et al., *Chemokine detection in the cerebral tissue of patients with posttraumatic brain contusions*. J Neurosurg, 2008. **108**(5): p. 958–962.
51. Lumpkins, K., et al., *Plasma levels of the beta chemokine regulated upon activation, normal T cell expressed, and secreted (RANTES) correlate with severe brain injury*. J Trauma, 2008. **64**(2): p. 358–361.
52. Nazari-Jahantigh, M., et al., *MicroRNA-155 promotes atherosclerosis by repressing Bcl6 in macrophages*. J Clin Invest, 2012. **122**(11): p. 4190–4202.
53. Butovsky, O., et al., *Targeting miR-155 restores abnormal microglia and attenuates disease in SOD1 mice*. Ann Neurol, 2015. **77**(1): p. 75–99.
54. O'Connell, R.M., et al., *MicroRNA-155 is induced during the macrophage inflammatory response*. Proc Natl Acad Sci U S A, 2007. **104**(5): p. 1604–1609.
55. Kerr, W.G., *Inhibitor and activator: dual functions for SHIP in immunity and cancer*. Ann N Y Acad Sci, 2011. **1217**: p. 1–17.
56. Gaudet, A.D., et al., *MicroRNAs: Roles in Regulating Neuroinflammation*. Neuroscientist, 2017: https://doi.org/10.1177/1073858417721150.

57. Stenvang, J., et al., *Inhibition of microRNA function by antimiR oligonucleotides*. Silence, 2012. **3**(1): p. 1.
58. Keck-Wherley, J., et al., *Abnormal microRNA expression in Ts65Dn hippocampus and whole blood: contributions to Down syndrome phenotypes*. Dev Neurosci, 2011. **33**(5): p. 451–467.
59. Woodbury, M.E., et al., *miR-155 Is Essential for Inflammation-Induced Hippocampal Neurogenic Dysfunction*. J Neurosci, 2015. **35**(26): p. 9764–9781.
60. Hu, R., et al., *miR-155 promotes T follicular helper cell accumulation during chronic, low-grade inflammation*. Immunity, 2014. **41**(4): p. 605–619.
61. Yuan, Z., et al., *TREM-1-accentuated lung injury via miR-155 is inhibited by LP17 nanomedicine*. Am J Physiol Lung Cell Mol Physiol, 2016. **310**(5): p. L426–L438.
62. Harmon, J.L., et al., *Striatal Mitochondrial Disruption following Severe Traumatic Brain Injury*. J Neurotrauma, 2017. **34**(2): p. 487–494.